

This is the accept manuscript of urena Polo, Jon Luzuriaga, Jagoba Iturri, Igor Irastorza, José Luis Toca-Herrera, Gaskon Ibarretxe, Fernando Unda, Jose-Ramon Sarasua, Jose Ramon Pineda, Aitor Larrañaga,  
Nanostructured scaffolds based on bioresorbable polymers and graphene oxide induce the aligned migration and accelerate the neuronal differentiation of neural stem cells, *Nanomedicine: Nanotechnology, Biology and Medicine*, Volume 31, 2021, 102314, ISSN 1549-9634, <https://doi.org/10.1016/j.nano.2020.102314>. Published by © 2020 Elsevier under CC BY-NC-ND licence <https://creativecommons.org/licenses/by-nc-nd/4.0/>

(<https://www.sciencedirect.com/science/article/pii/S1549963420301684>)

## Nanostructured Scaffolds Based on Bioresorbable Polymers and Graphene Oxide

### Induce the Aligned Migration and Accelerate the Neuronal Differentiation of Neural Stem Cells

Y. Polo<sup>a§</sup>, J. Luzuriaga<sup>b§</sup>, J. Iturri<sup>c</sup>, I. Irastorza<sup>b</sup>, J.L. Toca-Herrera<sup>c</sup>, G. Ibarretxe<sup>b</sup>, F. Unda<sup>b</sup>, J.R. Sarasua<sup>d</sup>, J.R. Pineda<sup>b,e#</sup> and A. Larrañaga<sup>d#</sup>

<sup>a</sup>Polimerbio SL, Donostia-San Sebastian, Spain.

<sup>b</sup>Department of Cell Biology and Histology, Faculty of Medicine and Nursing, University of the Basque Country (UPV/EHU), Leioa, Spain.

<sup>c</sup>Institute for Biophysics, Department of Nanobiotechnology, BOKU University of Natural Resources and Life Sciences, Vienna, Austria.

<sup>d</sup>Group of Science and Engineering of Polymeric Biomaterials (ZIBIO Group), Department of Mining, Metallurgy Engineering and Materials Science & POLYMAT, University of the Basque Country (UPV/EHU), Bilbao, Spain.

<sup>e</sup>Achucarro Basque Center for Neuroscience, University of the Basque Country (UPV/EHU), Leioa, Spain.

<sup>§</sup>These authors contributed equally to this work.

**#Corresponding Authors:** Aitor Larrañaga. Department of Mining, Metallurgy Engineering and Materials Science & POLYMAT, University of the Basque Country (UPV/EHU), Bilbao, Spain.

Telephone: +34 946 013 935

E-mail: [aitor.larranagae@ehu.eus](mailto:aitor.larranagae@ehu.eus)

ORCID: 0000-0002-2123-6069

Jose R. Pineda. Cell Signaling lab, University of the Basque Country (UPV/EHU), Leioa, Spain

Telephone: +34 946 013 218

E-mail: [joseramon.pinedam@ehu.eus](mailto:joseramon.pinedam@ehu.eus)

ORCID: 0000-0002-0900-7466

#### Funding sources

Basque Government (GV/EJ) Department of Education, Linguistic Politics and Culture (GIC 15/52, IT-927-16), MINECO «Ramón y Cajal» program RYC-2013-13450 (JRP), The University of The Basque Country (UPV/EHU) by GIU16/66, UFI 11/44, COLAB19/03 and IKERTU-2020.0155. GV/EJ, IT831-13, Hazitek ZE-2019/00012-IMABI and ELKARTEK KK-2019/00093. Polimerbio and Y. P. have a Bikaintek PhD grant (20-AF-W2-2018-00001) and J.L. has a UPV/EHU grant DOKBERRI 2019 (DOCREC19/49).

#### Conflict of interest

The authors declare that there is no conflict of interest.

**Word Count-Abstract:** 143

**Word Count-Manuscript (body text + figure legends):** 5048

**Number of Figures:** 8

**Number of References:** 58

## Abstract

1  
2  
3           Within the field of neural tissue engineering, there is a huge need for the  
4  
5 development of materials that promote the adhesion, aligned migration and  
6  
7 differentiation of stem cells into neuronal and supportive glial cells. In this study, we  
8  
9 have fabricated bioresorbable elastomeric scaffolds combining an ordered  
10  
11 nanopatterned topography together with a surface functionalization with graphene oxide  
12  
13 (GO) in mild conditions. These scaffolds allowed the attachment of murine neural stem  
14  
15 cells (NSCs) without the need of any further coating of its surface with extracellular  
16  
17 matrix adhesion proteins. The NSCs were able to give rise to both immature neurons  
18  
19 and supporting glial cells over the nanostructured scaffolds *in vitro*, promoting their  
20  
21 aligned migration in cell clusters following the nanostructured grooves. This system has  
22  
23 the potential to reestablish spatially oriented neural precursor cell connectivity,  
24  
25 constituting a promising tool for future cellular therapy including nerve tissue  
26  
27 regeneration.  
28  
29  
30  
31  
32  
33

## Keywords

34  
35  
36  
37  
38  
39           Micro- and nanopatterning, neural stem cells, migration, cell differentiation, graphene  
40  
41 oxide, biodegradable polymer.  
42  
43  
44  
45  
46  
47  
48  
49  
50  
51  
52  
53  
54  
55  
56  
57  
58  
59  
60  
61  
62  
63  
64  
65

## Background

1  
2  
3  
4  
5  
6  
7  
8  
9  
10  
11  
12  
13  
14  
15  
16  
17  
18  
19  
20  
21  
22  
23  
24  
25  
26  
27  
28  
29  
30  
31  
32  
33  
34  
35  
36  
37  
38  
39  
40  
41  
42  
43  
44  
45  
46  
47  
48  
49  
50  
51  
52  
53  
54  
55  
56  
57  
58  
59  
60  
61  
62  
63  
64  
65

Regeneration of the nervous system still remains very challenging due to its limited plasticity and poor ability to heal and recover its function after injury.<sup>1</sup> Hence, further research is necessary to develop effective strategies for a guided neural regeneration and reestablishment of the lost nerve connectivity.

Within the field of neural tissue regeneration, the discovery and/or optimization of biomaterials that fulfill the complex requirements for this specific biomedical application play a pivotal role. Much progress has been made in determining the ideal features a biomaterial should have for its use as a neural replacement graft, and in understanding the interactions of growing axons within these biomaterials; however, the regeneration levels induced by the biomaterial usually do not match those obtained by nerve tissue autografts and the development of new and effective nerve regeneration therapies is still an urgent clinical need.<sup>2,3</sup>

The biomaterials for nerve tissue regeneration should be biocompatible and biodegradable, while providing structural cues that promote oriented axon regeneration and guidance signals from extracellular matrix (ECM)-like components. Additionally, they should also present long-term storage capability and ease of handling/suturing.<sup>4-6</sup> One important aspect to take in consideration is that the ECM is more than just a structural component. Indeed, for stem cells in particular, both the topography and composition of the ECM are pivotal in instructing cell fate choices by selective contact guidance, promotion of cell adhesion and concentration of growth factors and/or signaling ligands to defined niches.<sup>7</sup> However, negative effects produced by an inappropriate choice of ECM can also be identified. For instance, an excess of the typically employed ECM adhesion protein laminin  $\alpha_2\beta_2\gamma_1$  (Lm211) can inhibit signaling

1 pathways required to initiate myelination.<sup>8</sup> Furthermore, laminin ECM proteins may  
2 represent a lethal risk if at some point resident and/or grafted cells became cancerous. It  
3  
4 has been demonstrated that laminin primes the proliferation of brain tumor cells such  
5  
6  
7  
8  
9  
10  
11  
12  
13  
14  
15  
16  
17  
18  
19  
20  
21  
22  
23  
24  
25  
26  
27  
28  
29  
30  
31  
32  
33  
34  
35  
36  
37  
38  
39  
40  
41  
42  
43  
44  
45  
46  
47  
48  
49  
50  
51  
52  
53  
54  
55  
56  
57  
58  
59  
60  
61  
62  
63  
64  
65

To overcome these challenges, the use of polymeric substrates that mimic the  
mechanical (e.g., elasticity, stiffness), geometrical and chemical features of the ECM  
has been described to satisfactorily promote the differentiation of stem cells towards  
neural lineages.<sup>10</sup> Among the available polymeric substrates, bioresorbable  
(co)polyesters based on L-lactide and  $\epsilon$ -caprolactone are of particular interest. These  
systems show inherent biodegradability, biocompatibility and the possibility to tune the  
mechanical properties and degradation rates depending on the specific application, via  
the precise control of the L-lactide-to- $\epsilon$ -caprolactone ratio and synthesis conditions  
(e.g., catalyst, reaction temperature and time).<sup>11-13</sup> Nevertheless, nowadays, polymeric  
devices are not just bioinert support materials for cell growth. To fit within the new  
discipline of materiobiology,<sup>14</sup> they also need to mimic the morphological,  
topographical and mechanical properties of the desired tissue.<sup>15</sup> To fulfill these  
requisites, nanopattern construction represents a promising strategy to endow the  
material surface with specific geometrical and mechanical signals. Nanopatterns can  
potentially elicit a stem cell response, as surface nanotopography could induce  
pronounced changes to cell shape, and consequently also in gene expression.<sup>16</sup> In this  
regard, the importance of nanotopography was shown on the differentiation of adult  
stem cells towards neuronal lineages, compared to unpatterned and micro-patterned

1 control surfaces.<sup>17</sup> Moreover, the combination of nanotopography with graphene  
2 derivatives (e.g., graphene oxide (GO), reduced graphene oxide (rGO)) has been shown  
3 to promote neuronal differentiation and axon alignment.<sup>18</sup> In the recent years, GO-based  
4 materials have been extensively explored as some of the most promising biomaterials  
5 for neural regeneration<sup>19</sup> thanks to their unique properties.<sup>20</sup>  
6  
7  
8  
9  
10

11  
12 However, there is still much to investigate regarding the impact of  
13 nanotopography and graphene derivatives on the mobility of the cells along the scaffold  
14 device, the *in situ* differentiation of stem cells into glial or neuronal cells and the  
15 necessary equilibrium between both pathways, to achieve a functional recovery of the  
16 neural tissue. Therefore, we have developed novel two-dimensional nanostructured  
17 tissue engineering scaffolds based on bioresorbable polymers and GO as a new  
18 alternative to promote the neurodifferentiation of murine neural stem cells (NSCs) and  
19 progenitors, which are competent to give rise to both mature neuronal and glial cells.  
20 The high efficiency shown by these nanopatterned scaffolds, even under long incubation  
21 periods compatible with usual differentiation protocols, turns them into an optimal and  
22 easy-to-produce tool.  
23  
24  
25  
26  
27  
28  
29  
30  
31  
32  
33  
34  
35  
36  
37  
38  
39  
40  
41  
42

## 43 **Methods**

### 44 *Fabrication of scaffolds*

45  
46  
47  
48 PURASORB PLC 7015 (Corbion, The Netherlands) (PLCL 7015) is a  
49 biodegradable copolymer of L-lactide and  $\epsilon$ -caprolactone in a 70/30 molar ratio, with a  
50 weight average molecular weight ( $M_w$ ) of 154.6 kDa and dispersity index (DI) of 2.10,  
51 as determined by gel permeation chromatography (GPC). For the fabrication of the  
52  
53  
54  
55  
56  
57  
58  
59  
60  
61  
62  
63  
64  
65

1 scaffolds, PLCL films of around 150  $\mu\text{m}$  were first obtained by compression moulding  
2 in a Collin P 200 E (Germany) hydraulic press at 175  $^{\circ}\text{C}$ . These films were subsequently  
3  
4 nanostructured by a thermo-pressing process at 190  $^{\circ}\text{C}$  and 20 N with the aid of a  
5  
6 commercially available silicon stamp (NIL Technology, Denmark) (period: 700 nm;  
7  
8 linewidth: 365 nm; depth: 350 nm) (Supplementary Figure 1). For the surface-  
9  
10 functionalization with GO, the nanostructured PLCL scaffolds were incubated in a 2  
11  
12 mg/ml dopamine-hydrochloride (cat# H8502, Sigma-Aldrich, Spain) solution in TRIS  
13  
14 Buffer (cat# T1503, Sigma-Aldrich, Spain) at pH = 8.5 for 1 h to form a homogeneous  
15  
16 layer of polydopamine (PDA). To eliminate the excess of PDA and reagents, the films  
17  
18 were thoroughly washed with distilled water. Afterwards, PDA-coated films were  
19  
20 incubated in a 0.25 mg/ml GO solution (cat# 947-768-1, Graphenea, Spain) for 30 min  
21  
22 to allow the deposition of GO on the surface of the nanostructured scaffolds. Finally, the  
23  
24 scaffolds were extensively washed with distilled water prior to their use and  
25  
26 characterization. Circular samples of 6 mm diameter were punched out for subsequent  
27  
28 characterization and cell culture studies. Details about the morphological and physico-  
29  
30 chemical characterization of the scaffolds can be found in the supplementary material.  
31  
32  
33  
34  
35  
36  
37  
38  
39  
40

#### 41 *Cell culture*

42  
43  
44 NSCs were obtained, cultured in Neurocult proliferation media and passaged as  
45  
46 previously described.<sup>7</sup> Cells were seeded at a density of either 10,000 or 5,000 cells per  
47  
48 scaffold. For the control assays, NSCs were seeded onto 12 mm coverslips either coated  
49  
50 with laminin or non-coated (L2020, Sigma, St. Louis, MO), as previously described.<sup>22</sup>  
51  
52 Cell differentiation was induced using Neurocult differentiation supplement (cat#  
53  
54 05752, Stem Cell Technologies, Vancouver, Canada) at 9:1 ratio, 2% B27 supplement  
55  
56 (cat# 17504044, Gibco, Waltham, MA USA), in the presence of 100 U/ml penicillin and  
57  
58  
59  
60  
61  
62  
63  
64  
65

1 150 µg/ml streptomycin antibiotics. Fresh medium was replaced every three days. Cell  
2 orientations were calculated by measuring the orientation angle of the leading edge  
3 relative to a common reference point using ImageJ software. Further detailed  
4 information about cell cultures, immunostaining protocols as well as scanning electron  
5 microscopy (SEM) observations and videorecording of NSCs can be found in the  
6 supplementary material section.  
7  
8  
9  
10  
11  
12  
13

### 14 *Statistical methods*

15  
16  
17 Comparisons between multiple groups were made using Kruskal-Wallis  
18 followed by Dunn's post hoc test or Holm-Sidak method. In turn, comparisons between  
19 only two groups were made using U-Mann Whitney test, where  $p < 0.05$  was considered  
20 as statistically significant. Results were presented as mean  $\pm$  SD or SEM (indicated  
21 accordingly). The number of independent experiments is shown in the respective figure  
22 legend.  
23  
24  
25  
26  
27  
28  
29  
30  
31  
32  
33  
34  
35  
36

## 37 **Results**

### 38 *PLCL scaffolds are successfully fabricated, nanostructured and functionalized*

39  
40  
41  
42  
43 The topography of the silicon stamp was faithfully replicated on the PLCL films,  
44 yielding nanostructured PLCL scaffolds with a well-defined grooved pattern (Figure 1,  
45 A). The surface of the scaffolds was characterized by ridges of  $496.5 \pm 29.8$  nm and  
46 grooves of  $203.3 \pm 22.8$  nm. For a more detailed morphological characterization, atomic  
47 force microscopy (AFM) was employed (Figure 1, B). As evidenced from these images,  
48 some ridges appeared slightly distorted, which can be ascribed to the soft mechanical  
49 behavior of this polymer at room temperature.<sup>24</sup> The subsequent surface  
50 functionalization with PDA did not have any detrimental effect on the observed  
51  
52  
53  
54  
55  
56  
57  
58  
59  
60  
61  
62  
63  
64  
65

1 nanotopography (Figure 1, A and B). The concentration of the initial dopamine  
2 hydrochloride solution and the reaction time were carefully controlled to avoid the  
3  
4 excessive deposition of PDA agglomerates that could deteriorate the native  
5  
6 nanostructured topography of the scaffolds (Supplementary Figure 3, A). This  
7  
8 nanostructured topography was also preserved after the final functionalization with GO  
9  
10 (Figure 1, A and B). Working at higher GO concentrations in this step resulted in the  
11  
12 excessive deposition of GO, which, again, covered some areas of the polymeric film  
13  
14 (Supplementary Figure 3, B). In the case of non-nanostructured PLCL scaffolds  
15  
16 (Supplementary Figure 4, A and B) a slight increase in the overall roughness was  
17  
18 observed as PDA and GO were deposited, similar to the results observed for the  
19  
20 nanostructured scaffolds.  
21  
22  
23  
24  
25  
26

27 To confirm the successful functionalization of the scaffolds with PDA and GO,  
28  
29 the samples were subjected to X-ray photoelectron spectroscopy (XPS), Raman  
30  
31 spectroscopy and AFM in force spectroscopy mode analysis. After PDA coating, an  
32  
33 increase (from 29 to 41%) of the contribution at 285.0 eV, that corresponds to C-C/C-H  
34  
35 bonds, was observed in the C 1s spectrum with respect to the pristine PLCL scaffold  
36  
37 (Figure 2, A). Additionally, in the N 1s spectra a peak centered at 400.0 eV appeared,  
38  
39 which can be ascribed to secondary and primary amine groups, and imine functionalities  
40  
41 from PDA. The differences in the XPS spectra after surface functionalization with GO  
42  
43 with respect to PDA-coated films was negligible and only a slight decrease (from 3.1 to  
44  
45 1.6%) in the nitrogen signal was detected.  
46  
47  
48  
49  
50  
51

52 Raman spectroscopy however, truly confirmed the presence of GO on the  
53  
54 surface of the PLCL scaffolds (Figure 2, B). The intensities of the D and G bands, which  
55  
56 are associated respectively to the disordered structure of graphene in  $sp^2$ -hybridized  
57  
58 carbon and stretching of the C-C bond in graphitic materials,<sup>25</sup> increased with the  
59  
60  
61  
62  
63  
64  
65



1 concentration of the employed GO solution for the incubation. Note that the D and G  
2 bands were not present in the scaffold incubated with a 0.25 mg/ml GO solution but in  
3  
4 the absence of PDA adlayer, which highlights the importance of the PDA coating for the  
5  
6 successful functionalization of the surface with GO. Subsequent experiments were  
7  
8 performed with the scaffolds functionalized with a GO concentration of 0.25 mg/ml,  
9  
10 which ensured a successful surface functionalization while preserving the native  
11  
12 nanotopography of the PLCL scaffolds.  
13  
14  
15  
16

17  
18 The employment of AFM in force spectroscopy mode enabled the quantitative  
19  
20 evaluation of the mechanical properties (adhesion) at the interface between cells and the  
21  
22 substrate. As can be observed in Figure 2, C, hydrophobic probes led to larger forces  
23  
24 than fibronectin-coated ones (used as control), independently of the substrate under  
25  
26 analysis. For the hydrophobic probes, the maximum adhesion value, together with the  
27  
28 corresponding adhesion work, decreased with the different coatings applied  
29  
30 (Supplementary Table 1). This could be explained by the higher hydrophobic character  
31  
32 of PLCL (WCA ~ 90-100°), in comparison with thin PDA (WCA ~ 50°), GO (WCA ~  
33  
34 15-30°) and laminin (< 10°) films which were gradually more hydrophilic. This behavior  
35  
36 highlights the fact that level-wise modification of PLCL took place satisfactorily, and  
37  
38 that just a few nanometers are enough to change the character of the interface.  
39  
40  
41  
42  
43  
44

45  
46 For fibronectin-coated colloids, and despite the much lower values calculated,  
47  
48 the different content of the substrate also led to a variation in the adhesion-related  
49  
50 response. In this case, forces of hydrophobic nature were not the dominant ones  
51  
52 anymore. Indeed, adhesion factors for bare PLCL suffered a 10-fold drop in comparison  
53  
54 with hydrophobic probe measurements (Figure 2, C and Supplementary Table 1). Here,  
55  
56 PDA-coated scaffolds appeared as the predominant ones while those containing GO on  
57  
58  
59  
60  
61  
62  
63  
64  
65

1 top presented lower affinity for fibronectin, although still higher than control laminin  
2 films. Therefore, the effective action of the surface modification is again confirmed.  
3  
4  
5  
6  
7

8  
9 *Neural stem cells and progenitors attach and align following nanopattern shape without*  
10 *the need of a laminin coating*  
11  
12  
13

14 Laminin has been extensively used for monolayer coating of NSC cultures. To  
15 test whether NSCs were able to adhere and survive to surfaces without laminin coating,  
16 5,000 NSCs were seeded into nanostructured and non-nanostructured scaffolds.  
17 Alternatively to laminin, GO was employed owing to its reported physico-chemical  
18 features to improve cell adhesion and neuronal differentiation.<sup>11,15</sup> Forty-five minutes  
19 after initial seeding, only nanostructured surfaces showed a clear cellular orientation and  
20 attachment as evidenced by the guided growth of the cell leading edge (Figure 3, A). We  
21 noticed that most of the adhered cells shared the same orientation following the surface  
22 nanopattern. A quantification representing the variation of angle measurements was  
23 performed and determined that 70% of the cells were perfectly aligned with  
24 nanostructured scaffolds functionalized with GO (NanoGO), meanwhile nanostructured  
25 scaffolds without GO functionalization (NanoPDA) showed a 67% of cells aligned with  
26 a variation of 30°. Non-nanostructured scaffolds had shorter leading edge processes with  
27 no preferential orientation (Figure 3, B). Two hours post-seeding, the length of the  
28 leading cellular process was determined. The cells seeded on NanoGO showed the  
29 maximal elongation with an average of  $32.45 \pm 6.74 \mu\text{m}$  while NanoPDA showed a  
30 reduced length to  $23.66 \pm 5.41 \mu\text{m}$ . On the contrary, the leading processes of the cells  
31 seeded on non-nanostructured scaffolds functionalized with GO (No NanoGO) were  
32  
33  
34  
35  
36  
37  
38  
39  
40  
41  
42  
43  
44  
45  
46  
47  
48  
49  
50  
51  
52  
53  
54  
55  
56  
57  
58  
59  
60  
61  
62  
63  
64  
65

1 smaller than without the functionalization (No NanoPDA) ( $13.74 \pm 1.29$  and  $23.86 \pm 9.19$   
2  $\mu\text{m}$  respectively;  $p < 0.001$  ANOVA, Supplementary Figure 5).  
3  
4

5 To test whether nanostructured scaffolds were able to guide the orientation and  
6 migration of NSCs for longer periods that are compatible with neuronal differentiation  
7 protocols, the experiment was repeated by allowing the seeded NSCs to grow for three  
8 days *in vitro* (DIV3) in proliferation medium. Afterwards, the culture medium was  
9 changed to differentiation medium to allow cellular neurodifferentiation. The culture  
10 was kept for another seven days (total DIV10, Figure 4, A). The nanostructured  
11 materials induced an oriented growth and migration of NSCs along the parallel grooves  
12 during the initial three days of culture, independently of the GO functionalization. Non-  
13 nanostructured surfaces only showed large spheroid-shaped cellular structures as in  
14 (non-coated glass control) standard free-floating neurosphere cultures (Figure 4, B). To  
15 further confirm the results and corroborate that 1) cells were aligning according to the  
16 nanograting axis and 2) the alignment could be maintained after cell differentiation,  
17 cells were seeded and allowed to attach in proliferation medium for 24 h. Thereafter, the  
18 medium was changed to induce cell differentiation and cells were fixed at DIV7 or  
19 DIV14. SEM analysis demonstrated the alignment of cell clusters following the  
20 nanostructured grooves both at DIV7 (Supplementary Figure 6, A) and DIV14  
21 (Supplementary Figure 6, B). Thus, NSCs grew aligned with the surface nanopattern in  
22 a timescale compatible with neural cell differentiation protocols.  
23  
24  
25  
26  
27  
28  
29  
30  
31  
32  
33  
34  
35  
36  
37  
38  
39  
40  
41  
42  
43  
44  
45  
46  
47  
48  
49  
50  
51

### 52 *Surface nanostructured grooves allow the oriented migration of neural stem and* 53 *progenitor cells* 54 55 56

57 Since cell migration is a critical factor for complete tissue regeneration (e.g.,  
58 wound healing), the next step was to assess the dynamics of cell growth and adhesion  
59  
60  
61  
62  
63  
64  
65

1 over the different biomaterials. Hence, NSCs were seeded on the scaffolds and  
2 videorecorded for 72 h to characterize its migratory properties. Cells cultured over  
3  
4 nanostructured scaffolds independently on the functionalization with GO (NanoPDA vs  
5 NanoGO) displayed a lower motility with respect to cells cultured over laminin (mean  
6  
7 velocity of  $12.67 \pm 1.54 \mu\text{m/h}$  (NanoPDA),  $15.23 \pm 1.17 \mu\text{m/h}$  (NanoGO) and  $26.49 \pm 0.68$   
8  
9  $\mu\text{m/h}$  (laminin control)), ( $p < 0.001$  One-way ANOVA, Figures 5, A and B and  
10  
11 Supplementary Video 1). Remarkably, the difference between GO presence and GO  
12  
13 absence conditions was not statistically significant ( $p < 0.075$ , One-way ANOVA, Figure  
14  
15 5, B). Persistence time characterizes the average time between significant changes in the  
16  
17 direction of a translocation of a cell.<sup>26–28</sup> This value allows a quantitative analysis of the  
18  
19 differences in migration behavior. The results are shown in the percentage of time. The  
20  
21 cells cultured on nanostructured NanoPDA and NanoGO scaffolds showed significantly  
22  
23 more persistence than the cells cultured on laminin control ( $35.81 \pm 19.19\%$  (NanoPDA)  
24  
25 and  $17.82 \pm 5.51\%$  (NanoGO) respect to  $7.31 \pm 1.42\%$  (laminin control)), ( $p < 0.001$ , One-  
26  
27 way ANOVA, Figure 5, C). According to these results, nanostructured scaffolds showed  
28  
29 an increased pausing time in comparison with those coated with laminin ( $98.81 \pm 0.96\%$   
30  
31 (NanoPDA),  $97.37 \pm 0.72\%$  (NanoGO) and  $91.14 \pm 1.31\%$  (laminin control)), ( $p < 0.001$ ,  
32  
33 One-way ANOVA, Figure 5, D). Also the total traveled distance for an interval of 8 h  
34  
35 was similar on nanostructured scaffolds NanoPDA and NanoGO and much higher in the  
36  
37 case of laminin control ( $40.79 \pm 35.89 \mu\text{m}$  (NanoPDA),  $68.59 \pm 16.95 \mu\text{m}$  (NanoGO), and  
38  
39  $316.91 \pm 45.01 \mu\text{m}$  (laminin control)), ( $p < 0.001$ , One-way ANOVA, Figure 5, E).  
40  
41  
42  
43  
44  
45  
46  
47  
48  
49  
50  
51  
52  
53  
54  
55  
56  
57  
58  
59  
60  
61  
62  
63  
64  
65

1  
2  
3  
4  
5  
6  
7  
8  
9  
10  
11  
12  
13  
14  
15  
16  
17  
18  
19  
20  
21  
22  
23  
24  
25  
26  
27  
28  
29  
30  
31  
32  
33  
34  
35  
36  
37  
38  
39  
40  
41  
42  
43  
44  
45  
46  
47  
48  
49  
50  
51  
52  
53  
54  
55  
56  
57  
58  
59  
60  
61  
62  
63  
64  
65

*Neural stem and progenitor cells cultured on nanostructured scaffolds are able to generate neuronal and astroglial lineage cells*

Another important aspect for neural tissue cell therapy is to preserve the capabilities to generate newborn neurons as well as their supportive glial cells. To check whether nanostructured scaffolds were permissive to the generation of both neuronal and astroglial lineage, NSCs were first kept for 24 h in proliferation medium and then switched to differentiation medium. At DIV7 with differentiation medium, both nanostructured and non-nanostructured scaffolds with or without GO were fixed for immunostaining. Neuroblasts are neuronal precursors with migratory properties that strongly express the protein doublecortin (DCX).<sup>29-31</sup> On the other hand, astrocytes are other abundant cells in the central nervous system that abundantly express glial acidic fibrillary protein (GFAP).<sup>32</sup> Double immunofluorescence against DCX and GFAP showed the presence of both these cell types on the nanostructured scaffolds (Figure 6). In the case of non-nanostructured scaffolds, due to the lack of adhesion, only few cells were counted on the immunostaining.

*NSC differentiation to astroglial lineage is accelerated by the presence of both nanostructured grooves and GO*

NSCs cultured with differentiation medium on laminin-coated coverslips progressively differentiate towards mature astroglial fates over time (Figure 7). The level of glia maturation can be determined as follows: i) immunostaining for GFAP and the absence of S100 $\beta$  (immature glia), ii) the presence of both markers (maturing glia) and iii) the absence of GFAP and presence of S100 $\beta$  (fully mature glia). In control (laminin-coating) conditions, GFAP positive cells increased over time from 0.64 $\pm$ 0.13% at DIV3 to 28.35 $\pm$ 3.13% at DIV10 (p<0.005, One-way ANOVA) (Figure 7). These cells

1 also presented a more intense GFAP+ staining with longer differentiation time. On the  
2 other hand, S100 $\beta$ + staining did not present such variation with values of 20.97 $\pm$ 1.48%  
3  
4 at DIV3 and 28.60 $\pm$ 7.07% at DIV10 ( $p > 0.99$ , One-way ANOVA). But the maturing glia  
5 presenting GFAP and S100 $\beta$  double stain, increased from 0.32 $\pm$ 0.08% to 7.92 $\pm$ 1.27%  
6  
7 from DIV3 to DIV10, showing the maturation of the cells over time ( $p < 0.05$ , One-way  
8 ANOVA). The astroglial differentiation of cells seeded on the nanostructured scaffolds  
9 showed a remarkable increase on the amount of GFAP positive cells at DIV3 respect to  
10 laminin: NanoPDA 75.25 $\pm$ 4.10%, NanoGO 99.02 $\pm$ 8.58%, laminin control 0.64 $\pm$ 0.13%  
11  
12 ( $p < 0.05$ , One-way ANOVA). Therefore, both, the nanopatterning and the presence of  
13 GO seemed to shorten the onset of the glial differentiation of NSCs. Also, the  
14 percentage of S100 $\beta$ + increased in all the scaffolds tested at DIV3, respect to laminin  
15 control: NanoPDA 35.84 $\pm$ 2.33%, NanoGO 71.94 $\pm$ 4.37% and laminin control  
16 20.97 $\pm$ 1.48% ( $p < 0.05$ , One-way ANOVA). Again, this quick maturation was more  
17 remarkable on the nanostructured scaffolds functionalized with GO. The amount of  
18 GFAP+/S100 $\beta$ + double stained cells was also higher on the nanostructured scaffolds  
19 tested, with respect to laminin control at DIV3: NanoPDA 33.96 $\pm$ 2.37%, NanoGO  
20 70.94 $\pm$ 6.37% and laminin control 0.32 $\pm$ 0.08% ( $p < 0.05$ , One-way ANOVA).

21  
22  
23  
24  
25  
26  
27  
28  
29  
30  
31  
32  
33  
34  
35  
36  
37  
38  
39  
40  
41  
42 It is also worth mentioning that the nanostructured scaffolds functionalized with  
43 GO, even though they showed the most rapid glial differentiation, the amount of  
44 GFAP+, S100 $\beta$ + and GFAP+/S100 $\beta$ + double positive population was reduced at DIV7  
45 (GFAP+ 12.07 $\pm$ 1.83%; S100 $\beta$ + 0.25 $\pm$ 0.10%; GFAP+/S100 $\beta$ + 0.25 $\pm$ 0.10%) ( $p < 0.05$ ,  
46 One-way ANOVA) and DIV10 (GFAP+ 4.33 $\pm$ 0.50%; S100 $\beta$ + 18.68 $\pm$ 1.29%;  
47 GFAP+/S100 $\beta$ + 2.98 $\pm$ 0.43%) ( $p < 0.05$ , One-way ANOVA) with respect to the values  
48 observed at DIV3 (GFAP+ 99.02 $\pm$ 8.58%; S100 $\beta$ + 71.94 $\pm$ 4.37%; GFAP+/S100 $\beta$ +  
49 70.94 $\pm$ 6.37%). On the other hand, the NanoPDA scaffolds also presented a lower  
50  
51  
52  
53  
54  
55  
56  
57  
58  
59  
60  
61  
62  
63  
64  
65

1 population (5.89±0.20%) of GFAP+ positive cells at DIV10 compared to laminin  
2 control (28.35±3.13%) (p<0.05, One-way ANOVA).  
3  
4  
5  
6  
7

8 *NSC differentiation to neuronal lineage is enhanced by the combination of*  
9 *nanostructured grooves and GO*  
10  
11

12  
13 NSCs cultured with differentiation medium on laminin-coated coverslips  
14 progressively differentiate towards mature neuronal fates over time, losing DCX and  
15 expressing instead NeuN (Figure 8). The level of neuronal maturation was determined  
16 by: i) immunostaining for DCX and the absence of the nuclear neuronal marker NeuN  
17 (immature neurons), ii) the presence of both markers (maturing neurons) and iii) the  
18 absence of DCX and presence of NeuN (fully mature neurons). In control laminin-  
19 coating conditions the DCX+ positive cell population dropped significantly from  
20 30.85±2.41% at DIV7 to 15.90±0.02% at DIV10 (p<0.05, One-way ANOVA). The  
21 percentage of maturing neurons co-expressing DCX+/NeuN+ was of 15.66±3.31% and  
22 14.46±2.05% for DIV7 and DIV10, respectively (p<0.108, One-way ANOVA). When  
23 we turned to evaluate mature cell differentiation over scaffolds, NanoPDA and NanoGO  
24 were found to enhance neurodifferentiation of the cells compared to laminin control. We  
25 found that both NanoGO and NanoPDA scaffolds increased the amount of NeuN+  
26 positive cells at DIV10, compared to laminin control. (NanoGO 90.41±0.20, NanoPDA  
27 96.72±3.06% and laminin control 28.62±1.30%). Furthermore, NanoGO scaffolds  
28 increased the number of NeuN+ positive cells with respect to both laminin control and  
29 NanoPDA at DIV7 (NanoGO 52.50±0.04%; NanoPDA 3.2±0.01% and laminin control  
30 18.46±3.20%) (p<0.05, One-way ANOVA), thus considerably shortening the time  
31 needed for complete neuronal differentiation (Figure 8). Remarkably, PDA-coated  
32 scaffolds (NanoPDA) were enough to increase DCX+ (49.10±1.47%) and NeuN+

1 (96.72±3.05%) cell populations at DIV10 even without a need of neither laminin nor  
2 GO compared to laminin ( $p<0.05$ , One-way ANOVA). The number of neurons co-  
3  
4 expressing DCX+/NeuN+ was significantly increased on the NanoPDA scaffolds at  
5  
6 DIV10, with respect to NanoGO and laminin control (NanoPDA 49.18±0.03%;  
7  
8 NanoGO 24.08±0.02% and laminin control 14.46±2.05%), ( $p<0.05$ , One-way ANOVA).  
9  
10 Overall, NanoGO scaffolds seemed to accelerate the most the NSC differentiation into  
11  
12 neuronal pathway.  
13  
14  
15  
16  
17  
18

## 19 **Discussion**

20  
21  
22 In the present study, we characterized a nanostructured scaffold able to support  
23  
24 the oriented alignment, growth, migration and differentiation of neural stem and  
25  
26 progenitor cells. Although the use of nanostructured scaffolds as a tool to promote cell  
27  
28 alignment and differentiation is well reported in bibliography from a conceptual  
29  
30 perspective, most of the studies either employ non-biodegradable substrates or complex  
31  
32 procedures for the fabrication of the scaffolds, which enormously limit their potential in  
33  
34 the biomedical field.<sup>16,33–36</sup> Besides, the fabrication and post-functionalization processes  
35  
36 are frequently performed in the presence of organic solvents that may induce a cytotoxic  
37  
38 effect if they are not completely eliminated.<sup>37</sup> Herein, we employed a fully  
39  
40 bioresorbable, FDA-approved polymeric material based on L-lactide and  $\epsilon$ -caprolactone  
41  
42 (70/30 molar ratio).<sup>38</sup> Thanks to its thermoplastic nature, the nanotopography of a  
43  
44 commercially available silicon stamp was easily and quickly replicated on the  
45  
46 polymeric film without the need of any organic solvent or complex processes, which  
47  
48 highlights the robustness, scalability and versatility of this methodology. Following this  
49  
50 solvent-free strategy, the post-functionalization of the nanostructured scaffolds was  
51  
52 achieved by exploiting the multiple interactions between PDA and virtually any  
53  
54  
55  
56  
57  
58  
59  
60  
61  
62  
63  
64  
65



1 substrate in slightly basic aqueous solutions.<sup>39</sup> First, the nanostructured scaffolds were  
2 coated with a thin and homogeneously distributed layer of PDA that preserves the native  
3 nanotopography of the original films. The PDA coating played a pivotal role in the  
4 subsequent functionalization with GO as demonstrated by the absence of GO on the  
5 surface of the scaffolds when PDA was not employed as an adlayer. This can be  
6 associated to several interactions between PDA and GO, including hydrogen bonding  
7 between amine and hydroxyl groups of PDA and GO respectively and  $\pi$ - $\pi$  stacking  
8 between catechol groups of PDA and the hexagonal lattice of GO.<sup>40</sup>  
9  
10  
11  
12  
13  
14  
15  
16  
17  
18  
19

20 The properties of these scaffolds offer the advantage of NSC adhesion without  
21 the need of a laminin coating. Additionally, the nanostructured scaffolds NanoGO and  
22 NanoPDA offered the advantage of cell alignment and elongation along the  
23 nanostructured grooves. Even though the induction of cell alignment and elongation  
24 according to a determined nanograting axis has been reported before,<sup>16,41,42</sup> we found  
25 that nanostructured scaffolds also allowed the directionality of cell migration along the  
26 nanostructured grooves. Thus, our strategy goes a step further allowing the possibility of  
27 creating migration paths of NSCs and their differentiated cell progeny that follow a  
28 determined orientation according to the desired nanopatterning.  
29  
30  
31  
32  
33  
34  
35  
36  
37  
38  
39  
40  
41  
42

43 Another important aspect to take in consideration is the effect of the scaffolds to  
44 enhance and accelerate neural differentiation. We found that nanostructured scaffolds  
45 are able to induce cell differentiation towards both neuronal and astroglial lineages.  
46 Moreover, they are able to induce the differentiation towards neuronal lineages at earlier  
47 times than those of the ECM adhesion protein laminin. In accordance with these results  
48 it has been reported before the induction of neurodifferentiation of stem cells thanks to a  
49 synthetic nanostructure.<sup>17</sup> Besides, we found an increase on GFAP+ positive cells at  
50 early stages in the nanostructured scaffolds NanoPDA and NanoGO. It has been  
51  
52  
53  
54  
55  
56  
57  
58  
59  
60  
61  
62  
63  
64  
65

1 reported before the positive GFAP staining of NSCs cultured from postnatal mouse  
2 forebrains,<sup>43</sup> so these results may indicate the presence of undifferentiated NSCs in the  
3 culture at DIV3 and 7 on the scaffolds. The amount of S100 $\beta$ + positive cells is also  
4 increased at DIV3 in NanoGO scaffolds and at DIV7 on NanoPDA scaffolds compared  
5 to laminin control. Interestingly, S100 $\beta$  is expressed in both mature astroglia and early  
6 oligodendrocyte precursor cells.<sup>44,45</sup> In agreement with previous works, we cannot  
7 exclude the possibility of S100 $\beta$ + oligodendroglial cells at DIV3 on NanoGO scaffolds  
8 compared to NanoPDA.<sup>46</sup>

9  
10  
11  
12  
13  
14  
15  
16  
17  
18  
19  
20 On the other hand, it has been previously reported that the presence of GO  
21 enhances cellular neurodifferentiation,<sup>47</sup> while the combination of GO with electrical  
22 stimulation induces NSC proliferation, neuronal differentiation and neurite elongation.<sup>39</sup>  
23 Although GO has been widely chosen instead of pure graphene due to its better  
24 capability for laminin assembly, not much data has been reported for the effects of GO-  
25 coated scaffolds without the use of ECM-like intermediates.<sup>61,62</sup> We found that laminin-  
26 free NanoGO scaffolds reduced the time cells need to express neuronal markers with  
27 respect to standard laminin coating and NanoPDA scaffolds. Thus, both nanopatterning  
28 and GO surface functionalization can be combined to enhance and accelerate neuronal  
29 differentiation. In agreement with our results, other works claimed that nanostructured  
30 rGO microfibers were able to offer an alternative substrate for NSC adhesion when  
31 compared with 2D graphene films, and an increasing neuronal differentiation but with  
32 only few astroglial cells surrounding the microfibers.<sup>50</sup> In agreement with this work of  
33 Guo et al, we observed that neuronal differentiation was boosted at DIV7 on the  
34 NanoGO scaffolds, at the expense of the astroglial population. However, it is well  
35 reported in literature that glial cells are necessary to support neuronal cells.<sup>51-54</sup>  
36 Astrocytes for example, cooperate with neurons on several levels, including

1 neurotransmitter trafficking and recycling, ion homeostasis, energy metabolism, and  
2 defense against oxidative stress.<sup>55,56</sup> Consequently, this faster differentiation may  
3  
4 provoke a mid-term reduction of viability probably by changes of compensatory  
5  
6 proportions of neurons and astroglial support. Following the same reasoning, GO has  
7  
8 also been previously reported as a potential cytotoxic agent in chicken embryos.<sup>57,58</sup>  
9  
10 However, we have not found a variation of apoptotic/pycnotic nuclei in  
11  
12 immunostainings experiments, neither retracting cell process nor cell blebbing after  
13  
14 SEM examination. This fact reinforces the arguments for the potential use of these  
15  
16 systems.  
17  
18  
19  
20  
21  
22  
23  
24

## 25 **Acknowledgments**

26  
27  
28 We would like to thank Jorge Fernandez (Polimerbio SL) for the support in this  
29  
30 project. SGIker technical services (UPV/EHU) are gratefully acknowledged for XPS  
31  
32 and Raman support. We would like to thank Ricardo Andrade and Alejandro Díez,  
33  
34 responsible of the High-Resolution Analytical Microscopy Service in Biomedicine  
35  
36 (SGIker UPV/EHU), for their invaluable help for the electron microscopy and cell  
37  
38 videorecording assistance. We would like to thank Laura Escobar for confocal  
39  
40 microscopy in the Achucarro Basque Center for Neuroscience Fundazioa and Fabrice  
41  
42 Cordelières (Bordeaux Imaging Center) for the macro developed for ImageJ.  
43  
44  
45  
46  
47  
48  
49  
50  
51  
52  
53  
54  
55  
56  
57  
58  
59  
60  
61  
62  
63  
64  
65

## References

- 1 Ahuja C. S., Nori S., Tetreault L., Wilson J., Kwon B., Harrop J. et al, Traumatic spinal cord injury-repair and regeneration, *Neurosurgery*. 2017, **80**:S9–S22. <https://doi.org/10.1093/neuros/nyw080>.
- 2 Gu X., Ding F., Yang Y., Liu J., Construction of tissue engineered nerve grafts and their application in peripheral nerve regeneration, *Prog. Neurobiol.* 2011, **93**:204–230. <https://doi.org/10.1016/j.pneurobio.2010.11.002>.
- 3 Rajaram A., Chen X. B., Schreyer D. J., Strategic design and recent fabrication techniques for bioengineered tissue scaffolds to improve peripheral nerve regeneration, *Tissue Eng. Part B Rev.* 2012, **18**:454–467. <https://doi.org/10.1089/ten.TEB.2012.0006>.
- 4 Deumens R., Bozkurt A., Meek M. F., Marcus M. A. E., Joosten E. A. J., Weis J. et al, Repairing injured peripheral nerves: bridging the gap, *Prog. Neurobiol.* 2010, **92**:245–276. <https://doi.org/10.1016/j.pneurobio.2010.10.002>.
- 5 Kehoe S., Zhang X. F., Boyd D., FDA approved guidance conduits and wraps for peripheral nerve injury: a review of materials and efficacy, *Injury*. 2012, **43**:553–572. <https://doi.org/10.1016/j.injury.2010.12.030>.
- 6 Spivey E. C., Khaing Z. Z., Shear J. B., Schmidt C. E., The fundamental role of subcellular topography in peripheral nerve repair therapies, *Biomaterials*. 2012, **33**:4264–4276. <https://doi.org/10.1016/j.biomaterials.2012.02.043>.
- 7 Pineda J. R., Daynac M., Chicheportiche A., Cebrian-Silla A., Felice K. S., Garcia-Verdugo J. M. et al, Vascular-derived TGF- $\beta$  increases in the stem cell niche and perturbs neurogenesis during aging and following irradiation in the adult mouse brain, *EMBO Mol. Med.* 2013, **5**:548–562. <https://doi.org/10.1002/emmm.201202197>.

- 1  
2  
3  
4  
5  
6  
7  
8  
9  
10  
11  
12  
13  
14  
15  
16  
17  
18  
19  
20  
21  
22  
23  
24  
25  
26  
27  
28  
29  
30  
31  
32  
33  
34  
35  
36  
37  
38  
39  
40  
41  
42  
43  
44  
45  
46  
47  
48  
49  
50  
51  
52  
53  
54  
55  
56  
57  
58  
59  
60  
61  
62  
63  
64  
65
- 8 Ghidinelli M., Poitelon Y., Shin Y. K., Ameroso D., Williamson C., Ferri C. et al, Laminin 211 inhibits protein kinase A in Schwann cells to modulate neuregulin 1 type III-driven myelination, *PLoS Biol.* 2017, **15**:e2001408. <https://doi.org/10.1371/journal.pbio.2001408>.
  - 9 Lathia J. D., Li M., Hall P.E., Gallagher J., Hale J.S., Wu Q. et al, Laminin alpha 2 enables glioblastoma stem cell growth, *Ann. Neurol.* 2012, **72**:766–778. <https://doi.org/10.1002/ana.23674>.
  - 10 Zhang S., Ma B., Liu F., Duan J., Wang S., Qiu J. et al, Polylactic acid nanopillar array-driven osteogenic differentiation of human adipose-derived stem cells determined by pillar diameter, *Nano Lett.* 2018, **18**:2243–2253. <https://doi.org/10.1021/acs.nanolett.7b04747>.
  - 11 Ramot Y., Nyska A., Markovitz E., Dekel A., Klaiman G., Zada M. H. et al, Long-term local and systemic safety of poly(l-lactide-co-epsilon-caprolactone) after subcutaneous and intra-articular implantation in rats, *Toxicol. Pathol.* 2015, **43**:1127–1140. <https://doi.org/10.1177/0192623315600275>.
  - 12 Fernández J., Larrañaga A., Etxeberria A., Sarasua J. R., Effects of chain microstructures and derived crystallization capability on hydrolytic degradation of poly(l-lactide/ε-caprolactone) copolymers, *Polym. Degrad. Stab.* 2013, **98**:481–489. <https://doi.org/10.1016/j.polymdegradstab.2012.12.014>.
  - 13 Fernández J., Larrañaga A., Etxeberria A., Wang W., Sarasua J. R., A new generation of poly(lactide/ε-caprolactone) polymeric biomaterials for application in the medical field, *J. Biomed. Mater. Res. A.* 2014, **102**:3573–3584. <https://doi.org/10.1002/jbm.a.35036>.

- 1  
2  
3  
4  
5  
6  
7  
8  
9  
10  
11  
12  
13  
14  
15  
16  
17  
18  
19  
20  
21  
22  
23  
24  
25  
26  
27  
28  
29  
30  
31  
32  
33  
34  
35  
36  
37  
38  
39  
40  
41  
42  
43  
44  
45  
46  
47  
48  
49  
50  
51  
52  
53  
54  
55  
56  
57  
58  
59  
60  
61  
62  
63  
64  
65
- 14 Li Y., Xiao Y., Liu C., The horizon of materiobiology: a perspective on material-guided cell behaviors and tissue engineering, *Chem. Rev.* 2017, **117**:4376–4421. <https://doi.org/10.1021/acs.chemrev.6b00654>.
  - 15 Mohammed D., Versaevel M., Bruyère C., Alaimo L., Luciano M., Vercruyse E., Innovative tools for mechanobiology: unraveling outside-in and inside-out mechanotransduction, *Front. Bioeng. Biotechnol.* 2019, **7**:162. <https://doi.org/10.3389/fbioe.2019.00162>.
  - 16 Silantyeva E. A., Nasir W., Carpenter J., Manahan O., Becker M. L., Willits R. K., Accelerated neural differentiation of mouse embryonic stem cells on aligned GYIGSR-functionalized nanofibers, *Acta Biomater.* 2018, **75**: 129–139. <https://doi.org/10.1016/j.actbio.2018.05.052>.
  - 17 Yim E. K., Pang S. W., Leong K. W., Synthetic nanostructures inducing differentiation of human mesenchymal stem cells into neuronal lineage, *Exp. Cell Res.* 2007, **313**:1820–1829. <https://doi.org/10.1016/j.yexcr.2007.02.031>.
  - 18 Solanki A., Chueng S. T. D., Yin P. T., Kappera R., Chhowalla M., Lee K. B., Axonal alignment and enhanced neuronal differentiation of neural stem cells on graphene-nanoparticle hybrid structures, *Adv. Mater. Deerfield Beach Fla.* 2013, **25**:5477–5482. <https://doi.org/10.1002/adma.201302219>.
  - 19 Baek S., Oh J., Song J., Choi H., Yoo J., Park G. Y. et al, Generation of Integration-Free Induced Neurons Using Graphene Oxide-Polyethylenimine, *Small. Ger.* 2017, **13**:1601993. <https://doi.org/10.1002/sml.201601993>.
  - 20 Bramini M., Alberini G., Colombo E., Chiacchiaretta M., DiFrancesco M. L., Maya-Vetencourt J. F. et al, Interfacing graphene-based materials with neural cells, *Front. Syst. Neurosci.* 2018, **12**: 1662-5137. <https://doi.org/10.3389/fnsys.2018.00012>.

- 1  
2  
3  
4  
5  
6  
7  
8  
9  
10  
11  
12  
13  
14  
15  
16  
17  
18  
19  
20  
21  
22  
23  
24  
25  
26  
27  
28  
29  
30  
31  
32  
33  
34  
35  
36  
37  
38  
39  
40  
41  
42  
43  
44  
45  
46  
47  
48  
49  
50  
51  
52  
53  
54  
55  
56  
57  
58  
59  
60  
61  
62  
63  
64  
65
- 21 Luzuriaga J., Pastor-Alonso O., Encinas J. M., Unda F., Ibarretxe G., Pineda J. R., Human dental pulp stem cells grown in neurogenic media differentiate into endothelial cells and promote neovasculogenesis in the mouse brain, *Front. Physiol.* 2019, **10**:347. <https://doi.org/10.3389/fphys.2019.00347>.
  - 22 Silvestre D. C., Pineda J. R., Hoffschir F., Studler J. M., Mouthon M. A., Pflumio F. et al, Alternative lengthening of telomeres in human glioma stem cells, *Stem Cells.* 2011, **29**:440–51. <https://doi.org/10.1002/stem.600>.
  - 23 Cordelières F. P., Petit V., Kumasaka M., Debeir O., Letort V., Gallagher S. J. et al, Automated Cell Tracking and Analysis in Phase-Contrast Videos (iTrack4U): Development of Java Software Based on Combined Mean-Shift Processes, *PLoS ONE.* 2013, **8**:81266. <https://doi.org/10.1371/journal.pone.0081266>.
  - 24 Fernández J., Etxeberria A., Ugartemendia J. M., Petisco S., Sarasua J. R., Effects of chain microstructures on mechanical behavior and aging of a poly(L-lactide-co- $\epsilon$ -caprolactone) biomedical thermoplastic-elastomer, *J. Mech. Behav. Biomed. Mater.* 2012, **12**:29–38. <https://doi.org/10.1016/j.jmbbm.2012.03.008>.
  - 25 Wu J. B., Lin M. L., Cong X., Liu H. N., Tan P. H., Raman spectroscopy of graphene-based materials and its applications in related devices, *Chem. Soc. Rev.* 2018, **47**:1822–1873. <https://doi.org/10.1039/C6CS00915H>.
  - 26 Dunn G. A., Characterising a kinesis response: time averaged measures of cell speed and directional persistence, *Agents Actions. Suppl.* 1983, **12**:14–33. [https://doi.org/10.1007/978-3-0348-9352-7\\_1](https://doi.org/10.1007/978-3-0348-9352-7_1).
  - 27 Othmer H. G., Dunbar S. R., Alt W., Models of dispersal in biological systems, *J. Math. Biol.* 1988, **26**:263–298. <https://doi.org/10.1007/bf00277392>.
  - 28 Gail M. H., Boone C. W., The locomotion of mouse fibroblasts in tissue culture, *Biophys. J.* 1970, **10**:980–993. [https://doi.org/10.1016/S0006-3495\(70\)86347-0](https://doi.org/10.1016/S0006-3495(70)86347-0).

- 1  
2  
3  
4  
5  
6  
7  
8  
9  
10  
11  
12  
13  
14  
15  
16  
17  
18  
19  
20  
21  
22  
23  
24  
25  
26  
27  
28  
29  
30  
31  
32  
33  
34  
35  
36  
37  
38  
39  
40  
41  
42  
43  
44  
45  
46  
47  
48  
49  
50  
51  
52  
53  
54  
55  
56  
57  
58  
59  
60  
61  
62  
63  
64  
65
- 29 van Strien M. E., van den Berge S. A., Hol E. M., Migrating neuroblasts in the adult human brain: a stream reduced to a trickle, *Cell Res.* 2011, **21**:1523–1525. <https://doi.org/10.1038/cr.2011.101>.
- 30 Inta D., Alfonso J., von Engelhardt J., Kreuzberg M. M., Meyer A. H., van Hooft J. A., Monyer H., Neurogenesis and widespread forebrain migration of distinct GABAergic neurons from the postnatal subventricular zone, *Proc. Natl. Acad. Sci. U. S. A.* 2008, **105**:20994–20999. <https://doi.org/10.1073/pnas.0807059105>.
- 31 Englund U., Björklund A., Wictorin K., Migration patterns and phenotypic differentiation of long-term expanded human neural progenitor cells after transplantation into the adult rat brain, *Brain Res. Dev. Brain Res.* 2002, **134**:123–141. [https://doi.org/10.1016/s0165-3806\(01\)00330-3](https://doi.org/10.1016/s0165-3806(01)00330-3).
- 32 Eng L. F., Ghirnikar R. S., Lee Y. L., Glial fibrillary acidic protein: GFAP-thirty-one years (1969-2000), *Neurochem. Res.* 2000, **25**:1439–1451. <https://doi.org/10.1023/a:1007677003387>.
- 33 Baranes K., Shevach M., Shefi O., Dvir T., Gold Nanoparticle-decorated scaffolds promote neuronal differentiation and maturation, *Nano Lett.* 2016, **16**:2916–2920. <https://doi.org/10.1021/acs.nanolett.5b04033>.
- 34 Lee J. M., Kang W. S., Lee K. G., Cho H. Y., Conley B., Ahrberg C. D. et al, Combinatorial biophysical cue sensor array for controlling neural stem cell fate, *Biosens. Bioelectron.* 2020, **156**:112125. <https://doi.org/10.1016/j.bios.2020.112125>.
- 35 Zhang S., Ma B., Liu F., Duan J., Wang S., Qiu J., Li D. et al, Polylactic acid nanopillar array-driven osteogenic differentiation of human adipose-derived stem cells determined by pillar diameter, *Nano Lett.* 2018, **18**:2243–2253. <https://doi.org/10.1021/acs.nanolett.7b04747>.



- 1  
2  
3  
4  
5  
6  
7  
8  
9  
10  
11  
12  
13  
14  
15  
16  
17  
18  
19  
20  
21  
22  
23  
24  
25  
26  
27  
28  
29  
30  
31  
32  
33  
34  
35  
36  
37  
38  
39  
40  
41  
42  
43  
44  
45  
46  
47  
48  
49  
50  
51  
52  
53  
54  
55  
56  
57  
58  
59  
60  
61  
62  
63  
64  
65
- 36 Bonaventura G., Iemmolo R., La Cognata V., Zimbone M., la Via F., Fragalà M. E. et al, Biocompatibility between silicon or silicon carbide surface and neural stem cells, *Sci. Rep.* 2019, **9**:1–13. <https://doi.org/10.1038/s41598-019-48041-3>.
- 37 Wang L., Liu X., Fu J., Ning X., Zhang M., Jiang Z. et al, Release of methylene blue from graphene oxide-coated electrospun nanofibrous scaffolds to modulate functions of neural progenitor cells, *Acta Biomater.* 2019, **88**:346–356. <https://doi.org/10.1016/j.actbio.2019.02.036>.
- 38 Park J. H., Lee B. K., Park S. H., Kim M. G., Lee J. W., Lee H. Y. et al, Preparation of Biodegradable and Elastic Poly( $\epsilon$ -caprolactone-co-lactide) Copolymers and Evaluation as a Localized and Sustained Drug Delivery Carrier, *Int J Mol Sci.* 2017, **18**:671. <https://doi.org/10.3390/ijms18030671>.
- 39 Lee H., Dellatore S. M., Miller W. M., Messersmith P. B., Mussel-inspired surface chemistry for multifunctional coatings, *Science* 2007, **318**:426-430. <https://doi.org/10.1126/science.1147241>.
- 40 Hwang S. H., Kang D., Ruoff R.S., Shin H.S., Park Y. B., Poly(vinyl alcohol) reinforced and toughened with poly(dopamine)-treated graphene oxide, and its use for humidity sensing, *ACS Nano*, 2014, **8**:6739-6747. <https://doi.org/10.1021/nn500504s>.
- 41 Solanki A., Chueng S. T. D., Yin P. T., Kappera R., Chhowalla M., Lee K. B., Axonal alignment and enhanced neuronal differentiation of neural stem cells on graphene-nanoparticle hybrid structures, *Adv. Mater.*, 2013, **25**:5477-5482. <https://doi.org/10.1002/adma.201302219>.
- 42 Pardo-Figuerez M., Martin N. R. W., Player D. J., Roach P., Christie S. D. R., Capel A. J. et al, Controlled arrangement of neuronal cells on surfaces

functionalized with micropatterned polymer brushes, *ACS Omega*. 2018, **3**:12383–12391. <https://doi.org/10.1021/acsomega.8b01698>.

- 43 Imura T., Kornblum H. I., Sofroniew M. V., The predominant neural stem cell isolated from postnatal and adult forebrain but not early embryonic forebrain expresses GFAP, *J. Neurosci.* 2003, **23**:2824–2832. <https://doi.org/10.1523/JNEUROSCI.23-07-02824.2003>.
- 44 Steiner J., Bernstein H. G., Bielau H., Berndt A., Brisch R., Mawrin C. et al, Evidence for a wide extra-astrocytic distribution of S100B in human brain, *BMC Neurosci.* 2007, **8**:1471-2202. <https://doi.org/10.1186/1471-2202-8-2>.
- 45 Deloulme J. C., Raponi E., Gentil B. J., Bertacchi N., Marks A., Labourdette G. et al, Nuclear expression of S100B in oligodendrocyte progenitor cells correlates with differentiation toward the oligodendroglial lineage and modulates oligodendrocytes maturation, *Mol. Cell. Neurosci.* 2004, **27**:453–465. <https://doi.org/10.1016/j.mcn.2004.07.008>.
- 46 Shah S., Yin P. T., Uehara T. M., Chueng S. T. D., Yang L., Lee K. B., Guiding Stem Cell Differentiation into Oligodendrocytes Using Graphene-Nanofiber Hybrid Scaffolds, *Adv. Mater.* 2014, **26**:3673–3680. <https://doi.org/10.1002/adma.201400523>.
- 47 Song J., Gao H., Zhu G., Cao X., Shi X., Wang Y., The preparation and characterization of polycaprolactone/graphene oxide biocomposite nanofiber scaffolds and their application for directing cell behaviors, *Carbon.* 2015, **95**:1039–1050. <https://doi.org/10.1016/j.carbon.2015.09.011>.
- 48 Fu C., Pan S., Ma Y., Kong W., Qi Z., Yang X., Effect of electrical stimulation combined with graphene-oxide-based membranes on neural stem cell proliferation

- and differentiation, *Artif. Cells Nanomed. Biotechnol.* 2019, **47**:1867–1876.  
<https://doi.org/10.1080/21691401.2019.1613422>.
- 49 Bei H. P., Yang Y., Zhang Q., Tian Y., Luo X., Yan M. et al, Graphene-based nanocomposites for neural tissue engineering, *Molecules.* 2019, **24**:30781759.  
<https://doi.org/10.3390/molecules24040658>.
- 50 Guo W., Qiu J., Liu J., Liu H., Graphene microfiber as a scaffold for regulation of neural stem cells differentiation, *Sci. Rep.* 2017, **7**:5678.  
<https://doi.org/10.1038/s41598-017-06051-z>.
- 51 Wilton D. K., Dissing-Olesen L., Stevens B., Neuron-glia signaling in synapse elimination, *Annu. Rev. Neurosci.* 2019, **42**:107–127.  
<https://doi.org/10.1146/annurev-neuro-070918-050306>.
- 52 He F., Sun Y. E., Glial cells more than support cells?, *Int. J. Biochem. Cell Biol.* 2007, **39**:661–665. <https://doi.org/10.1016/j.biocel.2006.10.022>.
- 53 Araque A., Navarrete M., Glial cells in neuronal network function, *Philos. Trans. R. Soc. B Biol. Sci.* (2010) **365**:2375–2381.  
<https://doi.org/10.1098/rstb.2009.0313>.
- 54 Barber C. N., Raben D. M., Lipid metabolism crosstalk in the brain: glia and neurons, *Front. Cell. Neurosci.* , 2019, **13**:212.  
<https://doi.org/10.3389/fncel.2019.00212>.
- 55 Bélanger M., Magistretti P. J., The role of astroglia in neuroprotection, *Dialogues Clin. Neurosci.* 2009, **11**:281–295.
- 56 Kim B. J., Choi J. Y., Choi H., Han S., Seo J., Kim J. et al, Astrocyte-encapsulated hydrogel microfibers enhance neuronal circuit generation, *Adv. Healthc. Mater.* 2020, **9**:1901072. <https://doi.org/10.1002/adhm.201901072>.

- 1  
2  
3  
4  
5  
6  
7  
8  
9  
10  
11  
12  
13  
14  
15  
16  
17  
18  
19  
20  
21  
22  
23  
24  
25  
26  
27  
28  
29  
30  
31  
32  
33  
34  
35  
36  
37  
38  
39  
40  
41  
42  
43  
44  
45  
46  
47  
48  
49  
50  
51  
52  
53  
54  
55  
56  
57  
58  
59  
60  
61  
62  
63  
64  
65
- 57 Sawosz E., Jaworski S., Kutwin M., Hotowy A., Wierzbicki M., M. Grodzik M. et al Toxicity of pristine graphene in experiments in a chicken embryo model, *Int. J. Nanomedicine*. 2014, **9**:3913–3922. <https://doi.org/10.2147/IJN.S65633>.
- 58 Chen Y., Hu X., Sun J., Zhou Q., Specific nanotoxicity of graphene oxide during zebrafish embryogenesis, *Nanotoxicology*. 2016, **10**:42–52. <https://doi.org/10.3109/17435390.2015.1005032>.

## Figure Legends

Figure 1. Morphological characterization of the nanostructured scaffolds.

(A) SEM and (B) AFM micrographs of nanostructured PLCL (Nano), nanostructured PLCL coated with PDA (NanoPDA) and further functionalized with GO (NanoGO). (C) AFM 3-dimensional micrograph and (D) SEM cross-section micrograph of a nanostructured PLCL scaffold. Scale bars, 2  $\mu\text{m}$ .

Figure 2. Surface characterization of the scaffolds.

(A) High resolution C 1s (top) and N 1s (bottom) XPS spectra of nanostructured PLCL (Nano), nanostructured PLCL coated with PDA (NanoPDA) and further functionalized with GO (NanoGO). (B) Raman spectra of NanoGO scaffolds at different concentrations of GO solution. (C) Mean adhesion force (left) and work of adhesion (right) values for FSi (white) and fibronectin-coated (grey) probes. The error bars correspond to the standard error of the mean (SEM).

Figure 3. Neural stem cells and progenitors align along the nanostructured grooves without a need of laminin coating.

(A) Brightfield microscopy images of NSCs forty-five minutes after seeding, showing the parallel alignment of cell elongations on nanostructured scaffolds. (B) Distribution of cell orientation measuring angle degrees around the mean ( $90^\circ$ ) in NanoGO (78 cells analyzed), NanoPDA (45 cells), No NanoGO (31 cells) and No NanoPDA (26 cells). Scale bars, 25  $\mu\text{m}$ .

1  
2  
3  
4  
5  
6  
7  
8  
9  
10  
11  
12  
13  
14  
15  
16  
17  
18  
19  
20  
21  
22  
23  
24  
25  
26  
27  
28  
29  
30  
31  
32  
33  
34  
35  
36  
37  
38  
39  
40  
41  
42  
43  
44  
45  
46  
47  
48  
49  
50  
51  
52  
53  
54  
55  
56  
57  
58  
59  
60  
61  
62  
63  
64  
65

Figure 4. Neural stem cells and progenitors align following the nanostructured grooves without the need of a laminin coating.

(A) Scheme of experimental design. (B) Images showing the evolution of NSC cultures over the different substrates with no ECM protein coating in any of them. Cells align during the initial three days following the nanostructured grooves and do not detach during one-week differentiation. Cultures with non-nanostructured grooves grow forming cell clusters without any preferential cell alignment. Control condition using a coverslip without any ECM protein coating shows that cells do not attach growing as neurospheres. Scale bars, 100  $\mu\text{m}$ .

Figure 5. Nanostructured grooves induce the guided migration and alignment of neural stem and progenitor cells.

(A) Videomicroscopy snapshots at 0, 24, 48 and 72 h post seeding in nanostructured scaffolds illustrates the dynamic process of the parallel cell alignment. On the contrary NSCs seeded on laminin-coated surfaces show a random distribution over time. (B) Mean cell velocity, (C) Cell persistence, (D) Pausing time and (E) Total traveled distance of the cells over the NanoPDA and NanoGO scaffolds compared to laminin control. Bars are shown as mean  $\pm$  SEM. Dots show individual data. \*\*\* $p < 0.001$ , Kruskal-Wallis One Way Analysis of Variance on Ranks. Scale bars, 50  $\mu\text{m}$ .

Figure 6. Neural stem and progenitor cells cultured on nanostructured scaffolds are able to generate neuronal and astroglial precursor cells.

Confocal microscopy images of DCX (neuroblasts) and GFAP (astrocytes) immunostaining on nanostructured surfaces. Aligned clusters containing neuronal and

1 glial lineage cells are observed at DIV7 after switch to differentiation medium. DAPI  
2 was used as a counterstain for cell nuclei. Scale bar, 75 $\mu$ m.  
3  
4  
5  
6

7 Figure 7. Both nanostructured grooves and GO accelerate the differentiation of neural  
8 stem and progenitor cells towards astroglial lineage.  
9

10  
11 (A) Double immunofluorescence for the astroglial lineage markers GFAP (red) and  
12 S100 $\beta$  (green) at DIV 3, 7 and 10 post-seeding in the different conditions. (B)  
13  
14 Quantification of the proportion of GFAP+ (C) S100 $\beta$ + and (D) GFAP+/S100 $\beta$ + double  
15 stained positive cells. \* $p < 0.05$  compared to laminin. \*\*\* $p < 0.001$  between the  
16 treatments NanoPDA and NanoGO, Holm-Sidak method One Way Analysis of Variance  
17 on Ranks. Scale bar, 50  $\mu$ m.  
18  
19  
20  
21  
22  
23  
24  
25  
26  
27

28 Figure 8. Both nanostructured grooves and GO accelerate the differentiation of neural  
29 stem and progenitor cells towards neuronal lineage.  
30

31  
32 (A) Double immunofluorescence for the neuronal lineage markers DCX (red) and NeuN  
33 (green) at DIV 3, 7 and 10 post-seeding in the different conditions. (B) Quantification of  
34 the proportion of DCX+, (C) NeuN+ and (D) DCX+/NeuN+ double stained positive  
35 cells. \* $p < 0.05$  compared to laminin. \*\*\* $p < 0.001$  between the treatments NanoPDA and  
36 NanoGO, Holm-Sidak method One Way Analysis of Variance on Ranks. Scale bar, 50  
37  $\mu$ m.  
38  
39  
40  
41  
42  
43  
44  
45  
46  
47  
48  
49  
50  
51  
52  
53  
54  
55  
56  
57  
58  
59  
60  
61  
62  
63  
64  
65

# Figures

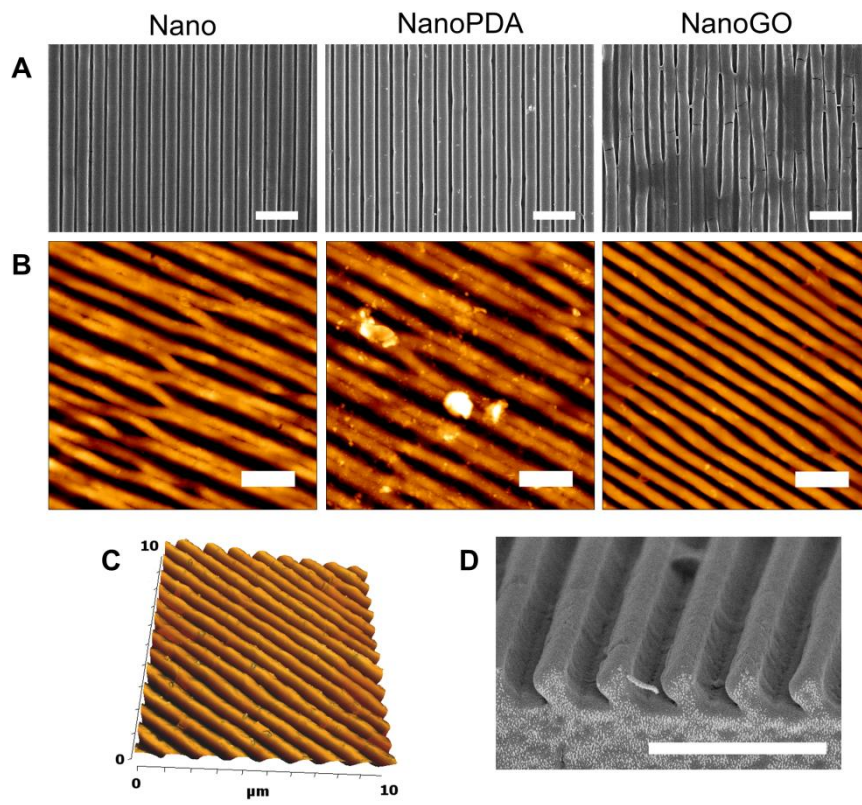


Figure 1



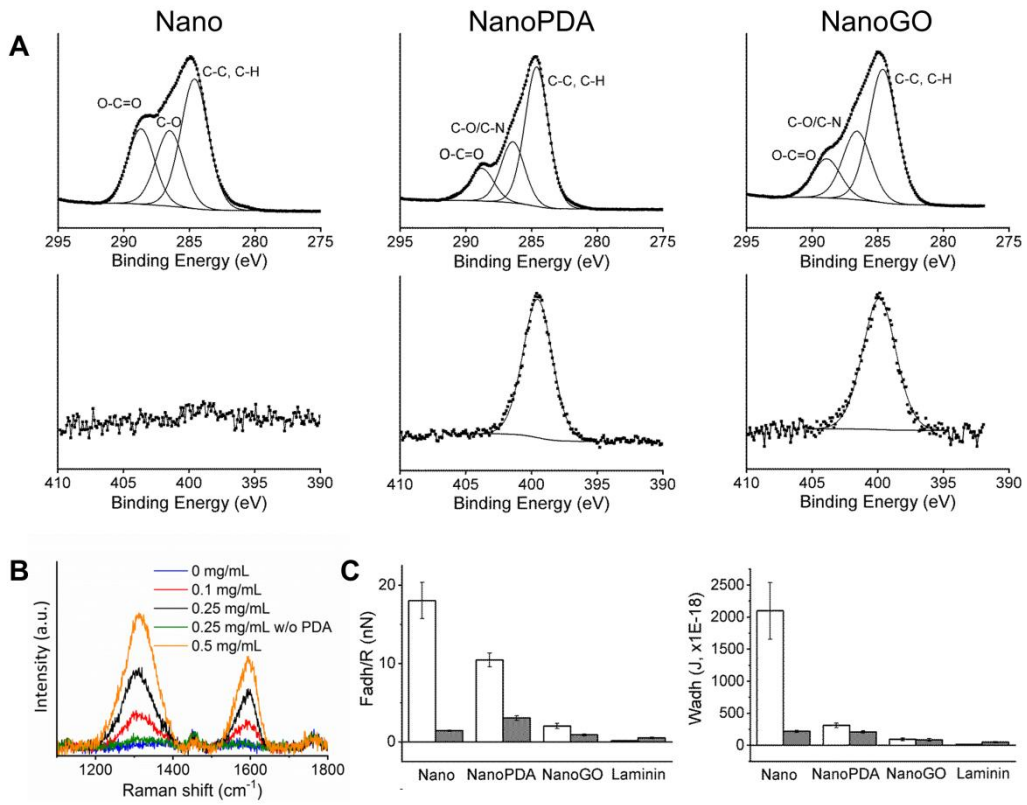


Figure 2

1  
2  
3  
4  
5  
6  
7  
8  
9  
10  
11  
12  
13  
14  
15  
16  
17  
18  
19  
20  
21  
22  
23  
24  
25  
26  
27  
28  
29  
30  
31  
32  
33  
34  
35  
36  
37  
38  
39  
40  
41  
42  
43  
44  
45  
46  
47  
48  
49  
50  
51  
52  
53  
54  
55  
56  
57  
58  
59  
60  
61  
62  
63  
64  
65

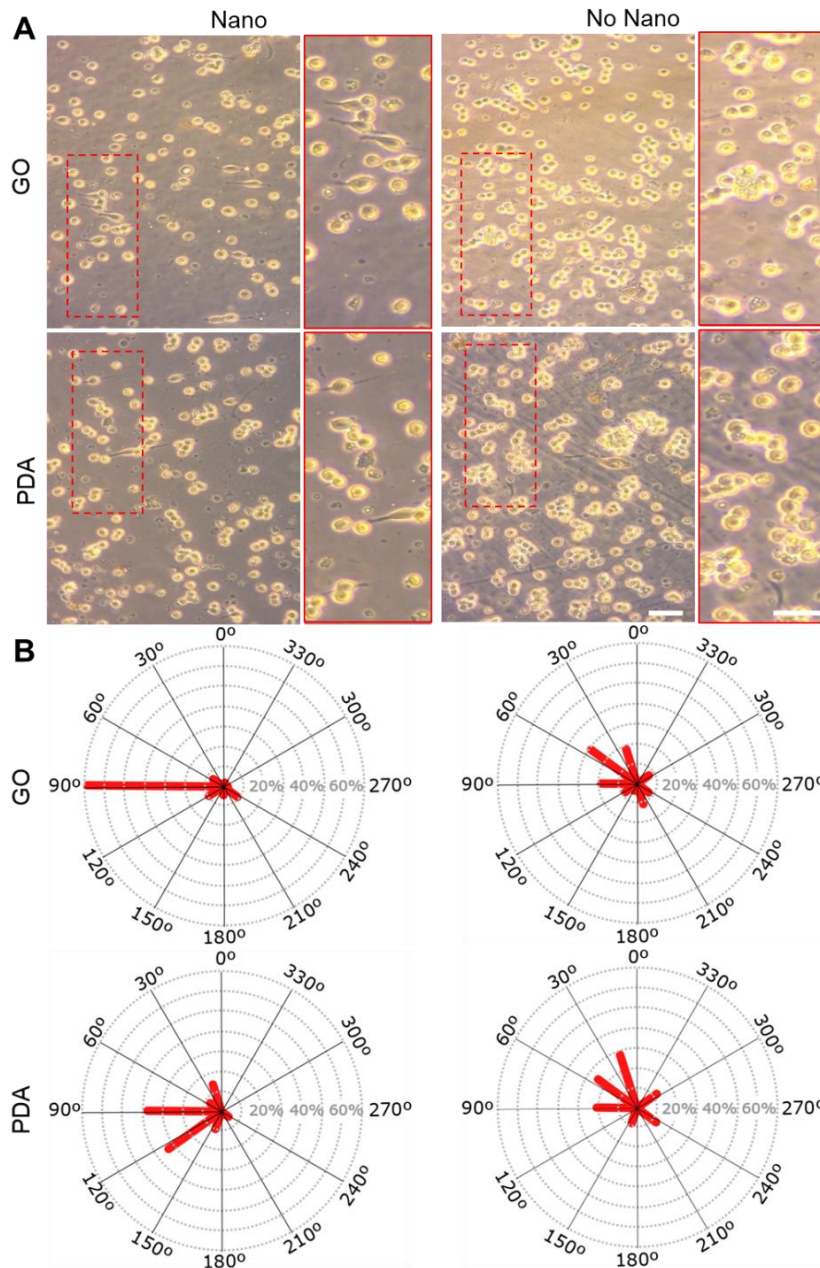


Figure 3

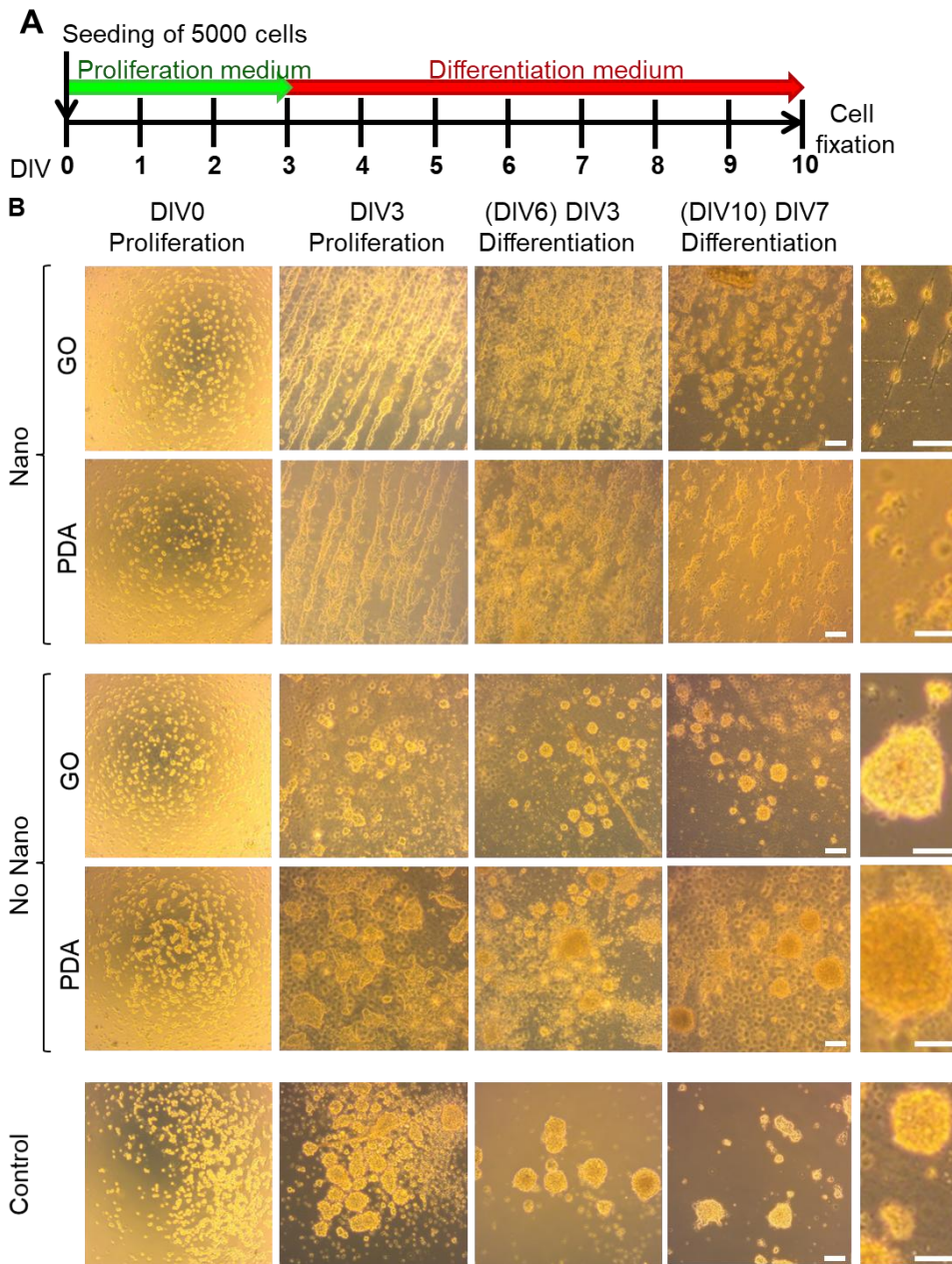


Figure 4

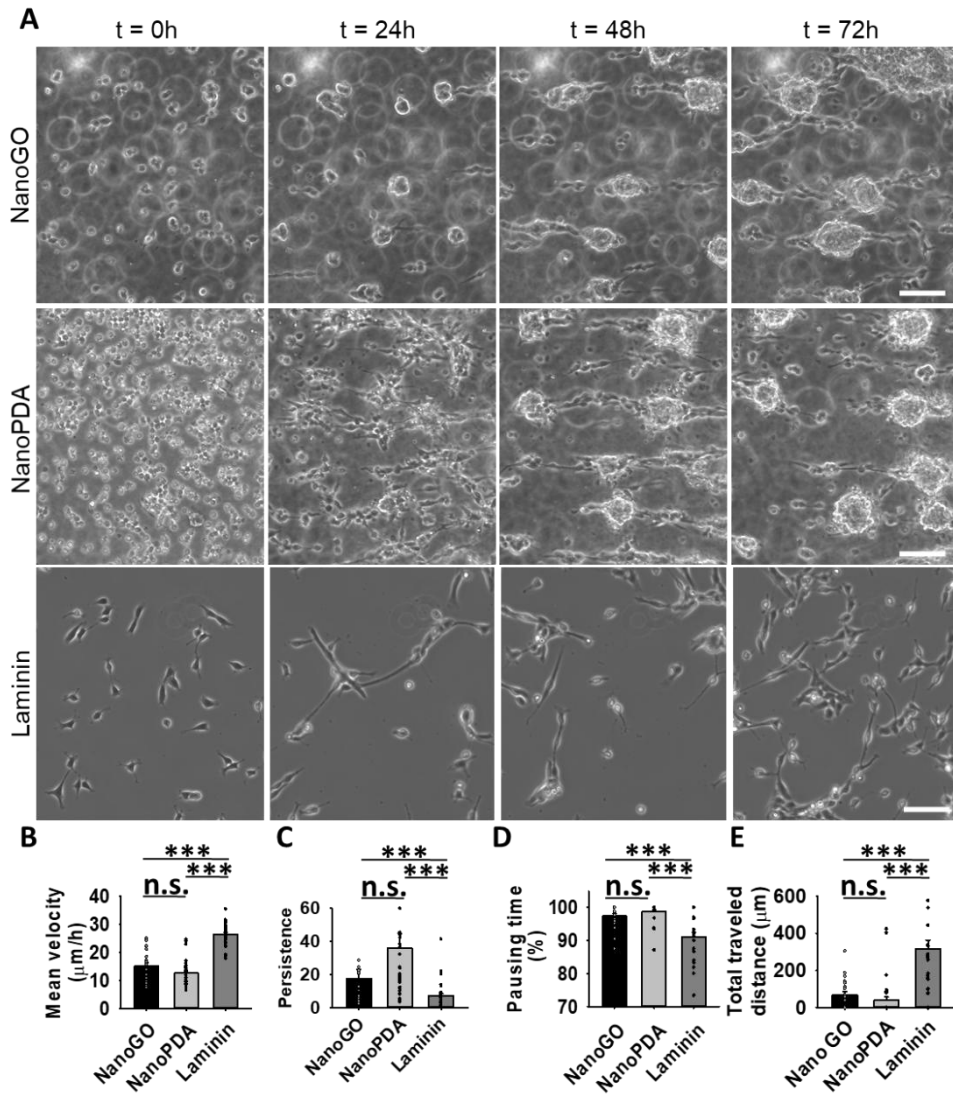


Figure 5



1  
2  
3  
4  
5  
6  
7  
8  
9  
10  
11  
12  
13  
14  
15  
16  
17  
18  
19  
20  
21  
22  
23  
24  
25  
26  
27  
28  
29  
30  
31  
32  
33  
34  
35  
36  
37  
38  
39  
40  
41  
42  
43  
44  
45  
46  
47  
48  
49  
50  
51  
52  
53  
54  
55  
56  
57  
58  
59  
60  
61  
62  
63  
64  
65

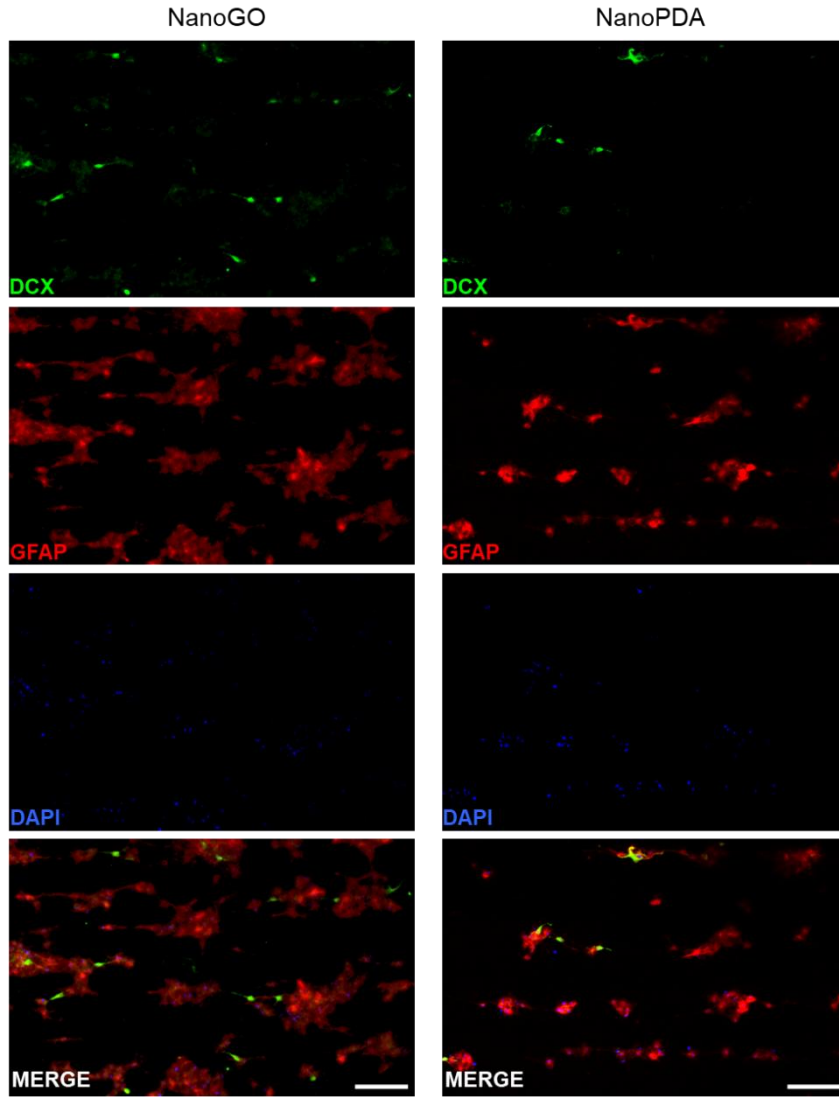


Figure 6

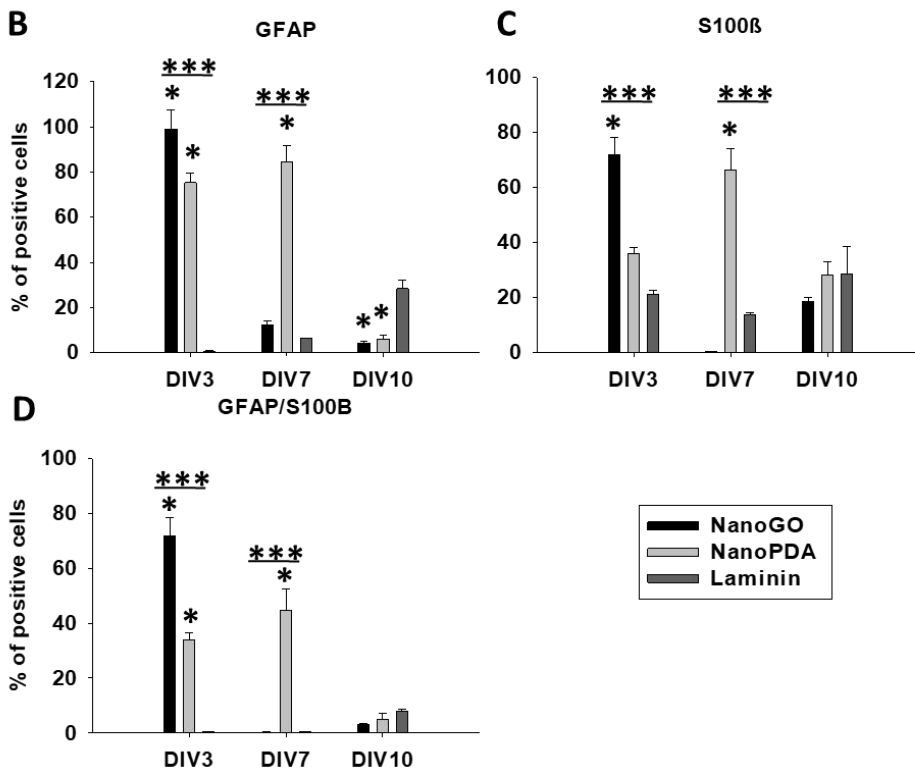
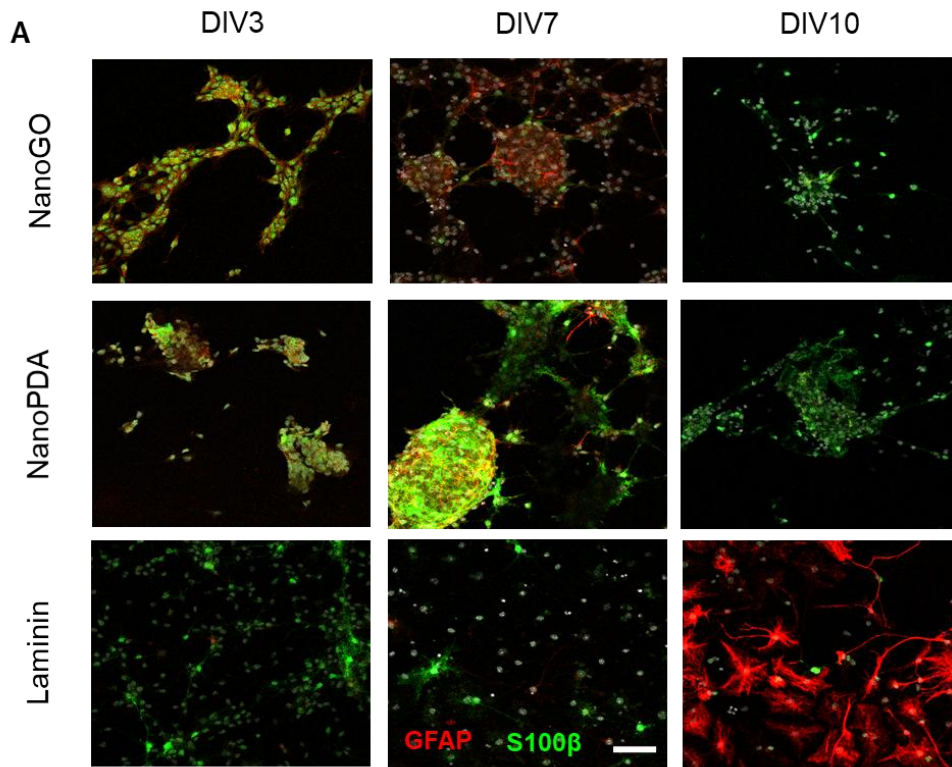


Figure 7

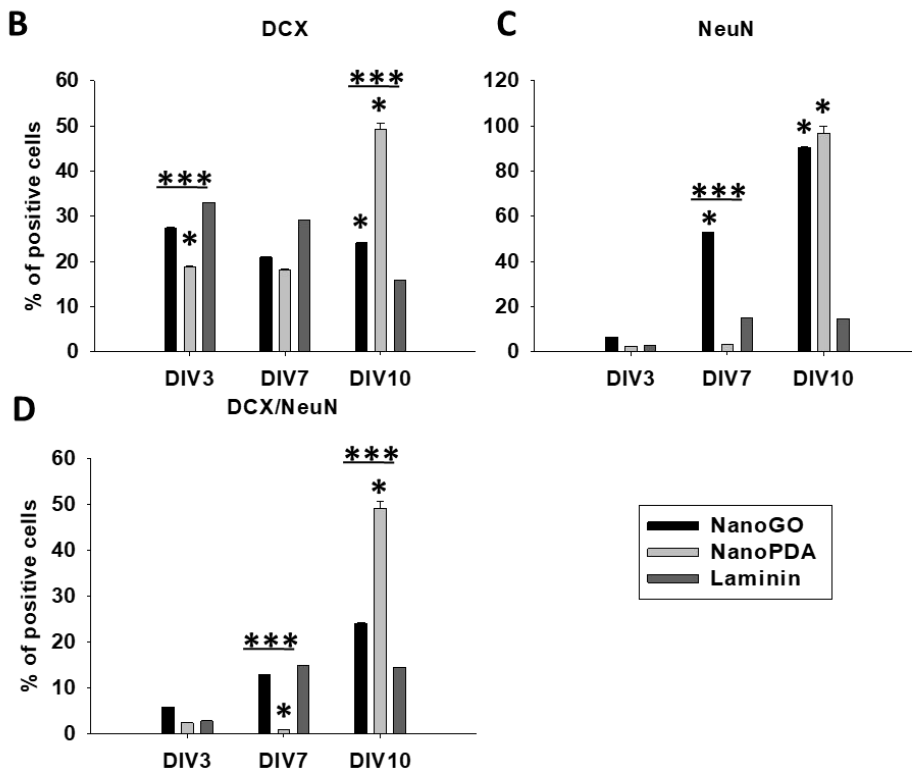
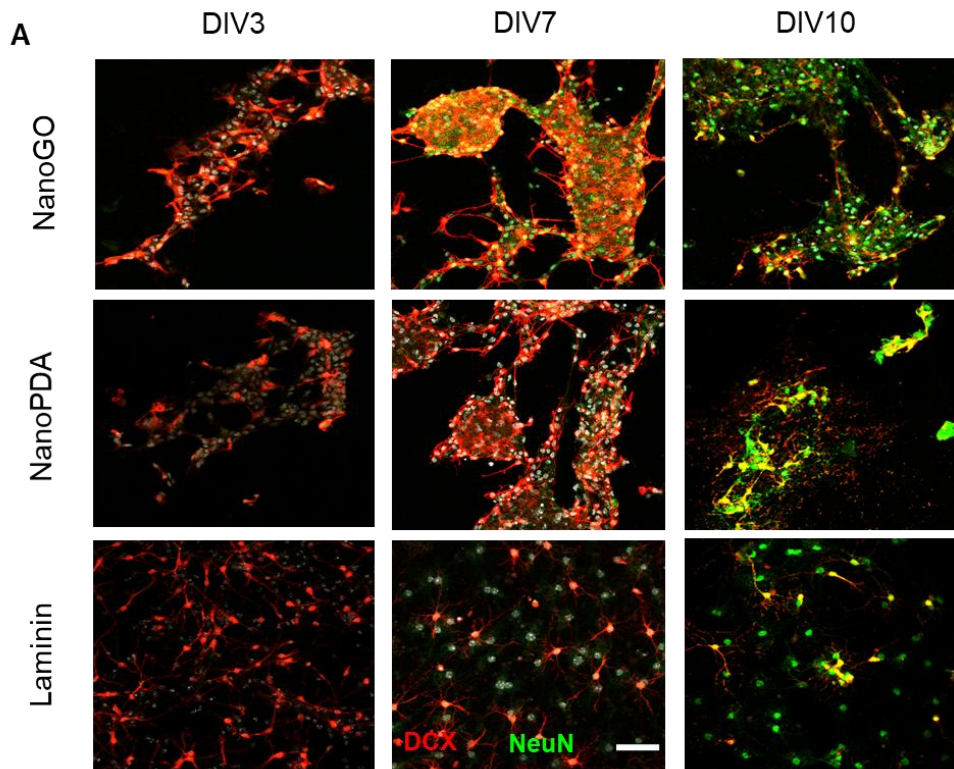


Figure 8

**Supplementary video**

[Click here to download Video: Supplemental video 1.avi](#)



**Supplementary Material**

[Click here to download Supplementary Material: Supplementary Material.docx](#)

### Highlights

- Thermoplastic nanopatterning of FDA-approved elastomeric bioresorbable polymer.
- Polydopamine-mediated surface functionalization with graphene oxide.
- Migration paths for neural stem and progenitor cells are created.
- Fast and efficient stem cell differentiation towards neuronal lineages.